WILEY

Online Proofing System

1. Corrections should be marked with the Adobe Annotation & Comment Tools below:

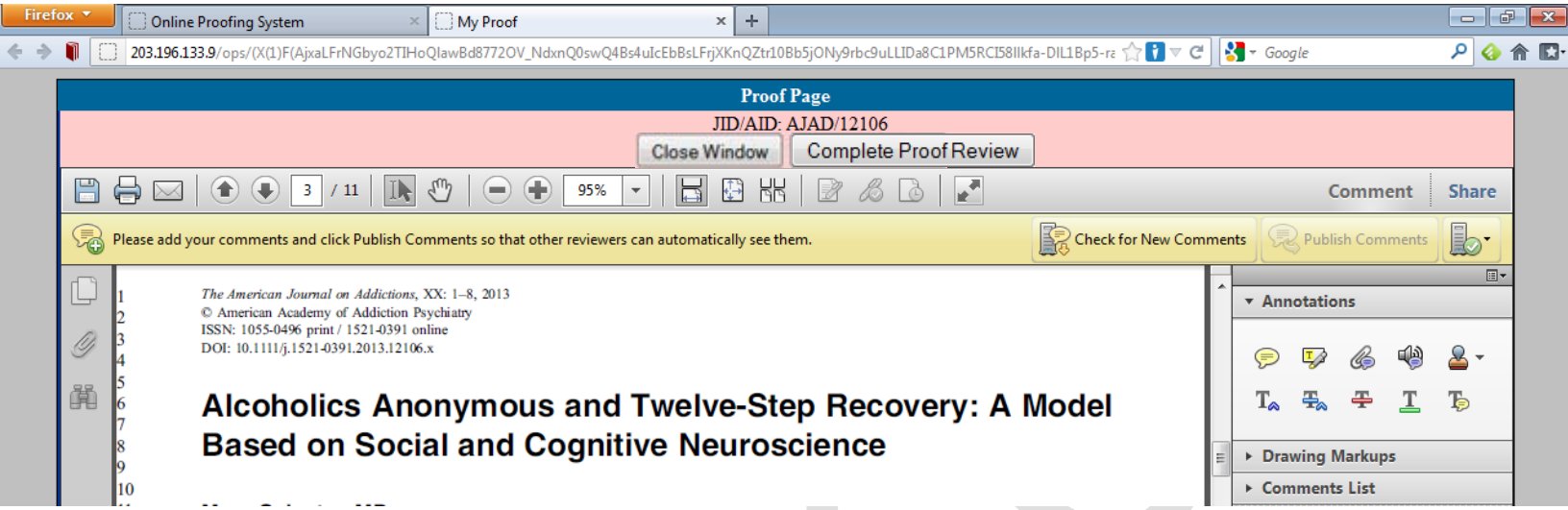

2. To save your proof corrections, click the 'Publish Comments' button. Publishing your comments saves the marked up version of your proof to a centralized location in Wiley's Online Proofing System. Corrections don't have to be marked in one sitting – you can publish corrections and log back in at a later time to add more.

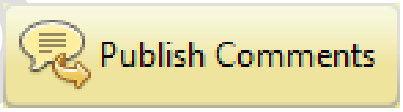

3. When your proof review is complete we recommend you download a copy of your annotated proof for reference in any future correspondence concerning the article before publication. You can do this by clicking on the icon to the right of the 'Publish Comments' button and selecting 'Save as Archive Copy…'.

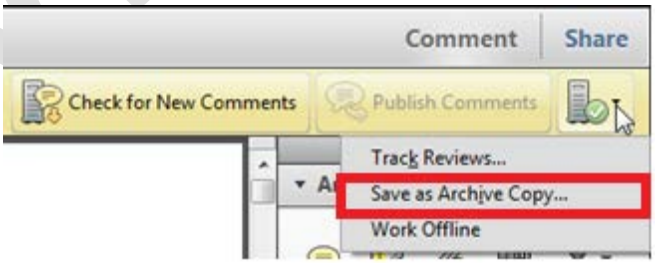

4. When your proof review is complete and you are ready to send corrections to the publisher click the 'Complete Proof Review' button that appears above the proof in your web browser window. Do not click the 'Complete Proof Review' button without replying to any author queries found on the last page of your proof. Incomplete proof reviews will cause a delay in publication. **Note: Once you click 'Complete Proof Review' you will not be able to mark any further comments or corrections**.

Firefox, Chrome, Safari Users

If your PDF article proof opens in any PDF viewer other than Adobe Reader or Adobe Acrobat, you will not be able to mark corrections and query responses, nor save them. To mark and save corrections, please follow these instructions to disable the built-in browser PDF viewers in Firefox, Chrome, and Safari so the PDF article proof opens in Adobe within a Firefox or Chrome browser window.

USING e-ANNOTATION TOOLS FOR ELECTRONIC PROOF CORRECTION

Required software to e-Annotate PDFs: Adobe Acrobat Professional or Adobe Reader (version 8.0 or above). (Note that this document uses screenshots from Adobe Reader X)
The latest version of Acrobat Reader can be downloaded for free at: http://get.adobe.com/reader/

Once you have Acrobat Reader open on your computer, click on the Comment tab at the right of the toolbar:

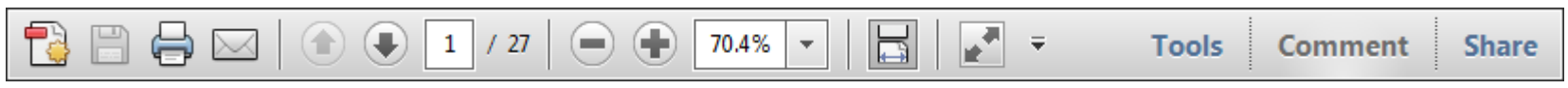

This will open up a panel down the right side of the document. The majority of tools you will use for annotating your proof will be in the Annotations section, pictured opposite. We've picked out some of these tools below:

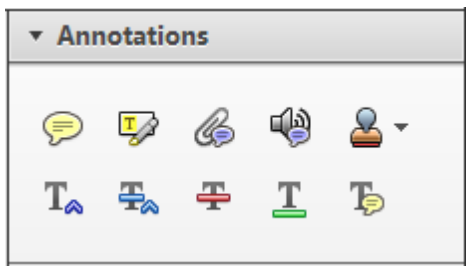

1. Replace (Ins) Tool – for replacing text.

Strikes a line through text and opens up a text box where replacement text can be entered.

How to use it

- Highlight a word or sentence.
- Click on the Replace (Ins) icon in the Annotations section.
- Type the replacement text into the blue box that appears.

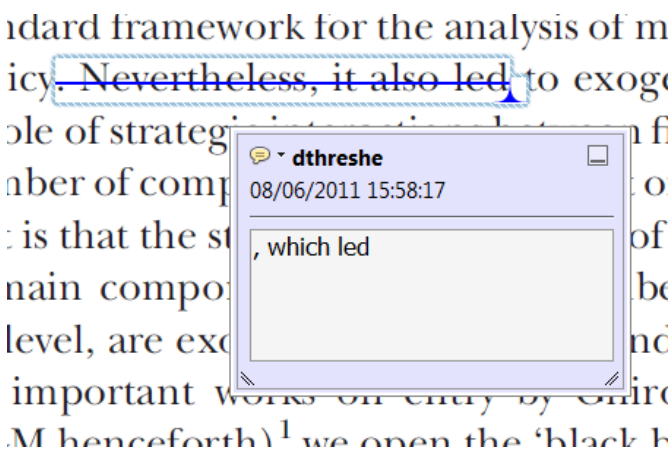

2. Strikethrough (Del) Tool – for deleting text.

Strikes a red line through text that is to be deleted.

How to use it

- Highlight a word or sentence.
- Click on the Strikethrough (Del) icon in the Annotations section.

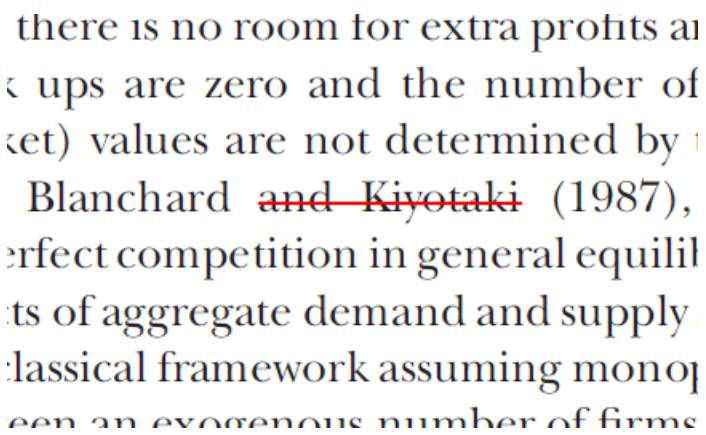

3. Add note to text Tool – for highlighting a section to be changed to bold or italic.

Highlights text in yellow and opens up a text box where comments can be entered.

How to use it

- Highlight the relevant section of text.
- Click on the Add note to text icon in the Annotations section.
- Type instruction on what should be changed regarding the text into the yellow box that appears.

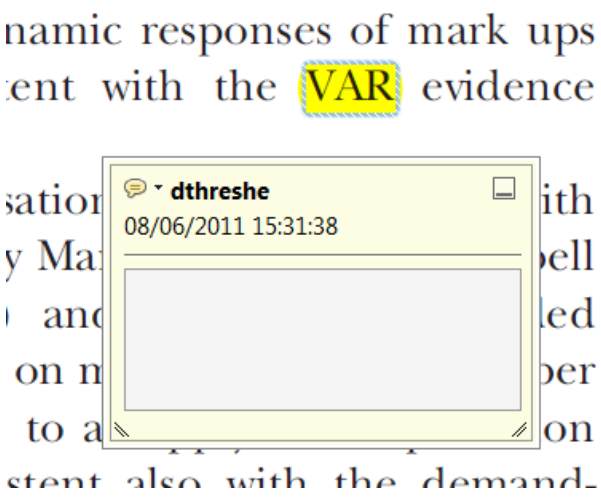

4. Add sticky note Tool – for making notes at specific points in the text.

Marks a point in the proof where a comment needs to be highlighted.

How to use it

- Click on the Add sticky note icon in the Annotations section.
- Click at the point in the proof where the comment should be inserted.
- Type the comment into the yellow box that appears.

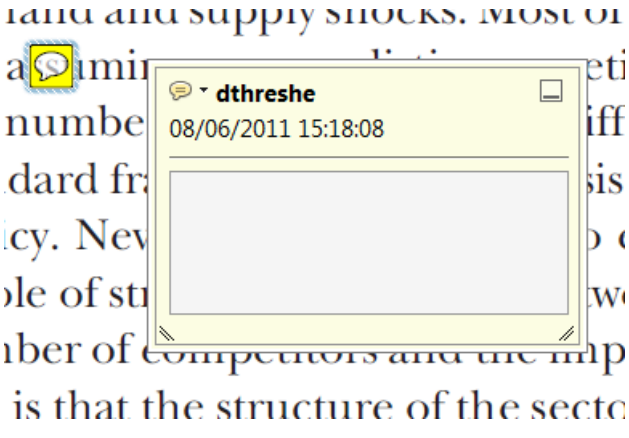

5. Attach File Tool – for inserting large amounts of text or replacement figures.

Inserts an icon linking to the attached file in the appropriate pace in the text.

How to use it

- Click on the Attach File icon in the Annotations section.
- Click on the proof to where you'd like the attached file to be linked.
- Select the file to be attached from your computer or network.
- Select the colour and type of icon that will appear in the proof. Click OK.

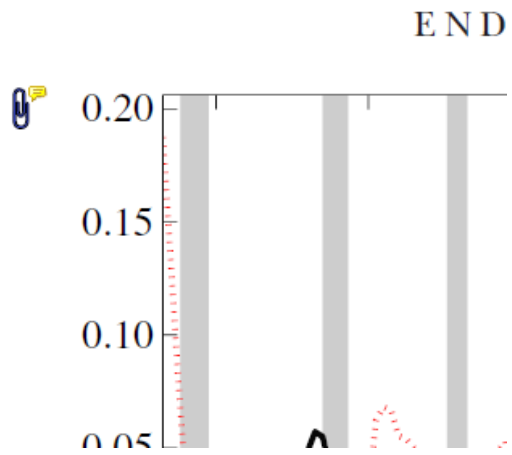

6. Add stamp Tool – for approving a proof if no corrections are required.

Inserts a selected stamp onto an appropriate place in the proof.

How to use it

- Click on the Add stamp icon in the Annotations section.
- Select the stamp you want to use. (The Approved stamp is usually available directly in the menu that appears).
- Click on the proof where you'd like the stamp to appear. (Where a proof is to be approved as it is, this would normally be on the first page).

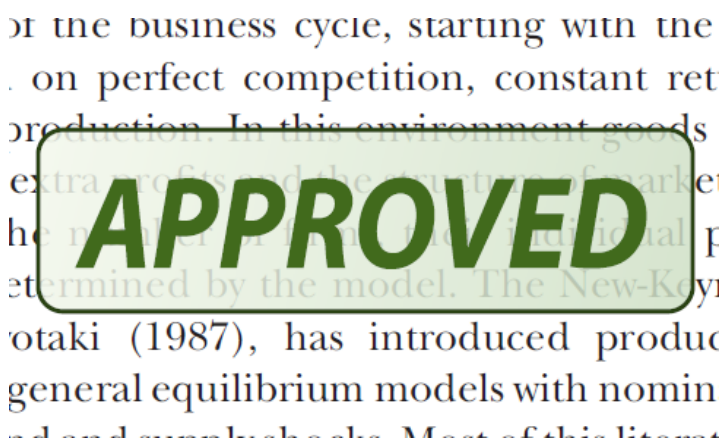

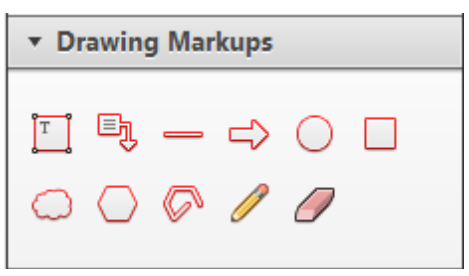

7. Drawing Markups Tools – for drawing shapes, lines and freeform annotations on proofs and commenting on these marks.

Allows shapes, lines and freeform annotations to be drawn on proofs and for comment to be made on these marks..

How to use it

- Click on one of the shapes in the Drawing Markups section.
- Click on the proof at the relevant point and draw the selected shape with the cursor.
- To add a comment to the drawn shape, move the cursor over the shape until an arrowhead appears.
- Double click on the shape and type any text in the red box that appears.

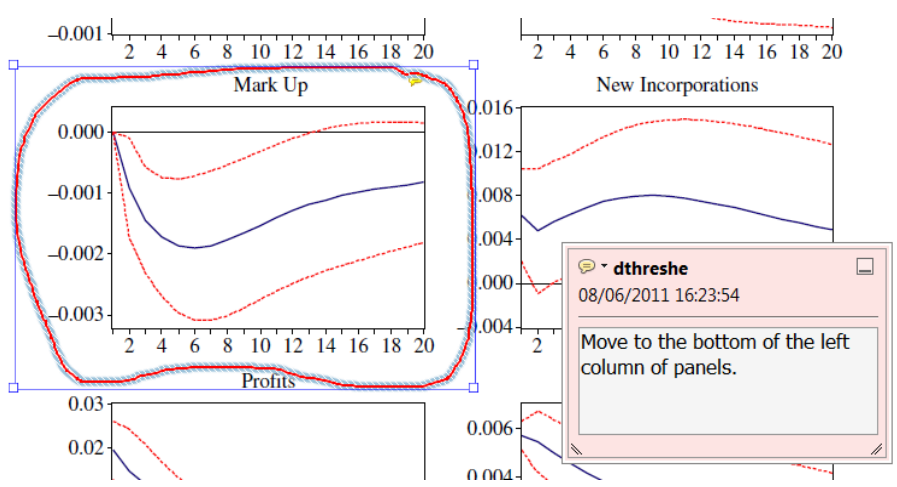

For further information on how to annotate proofs, click on the Help menu to reveal a list of further options:

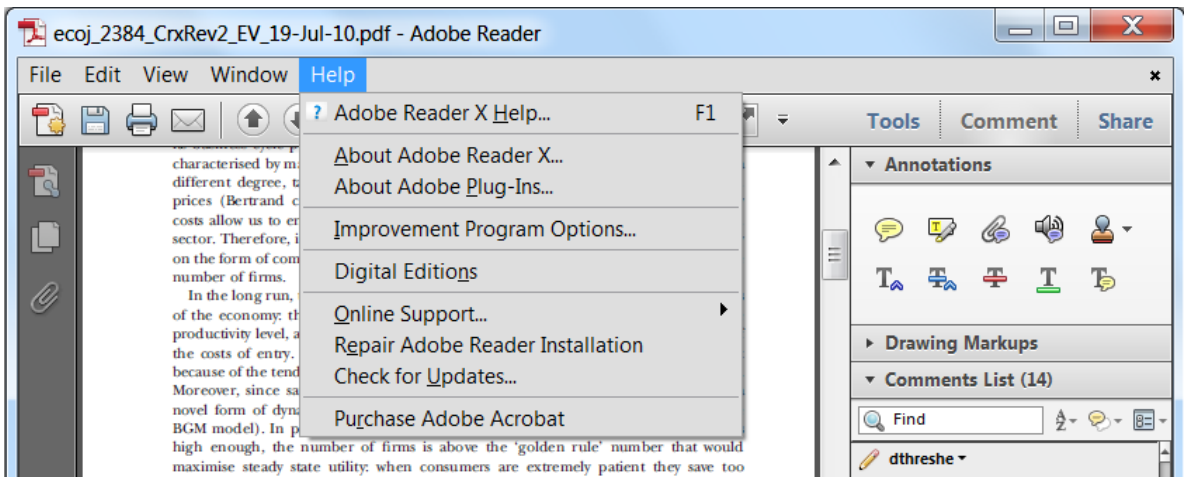

Role of Oxygen as a Regulator of Stem Cell Fate During the Spontaneous Repair of Osteochondral Defects

Adam O'Reilly,[1,2] Daniel J. Kelly[1,2,3]

[1]Trinity Centre for Bioengineering, Trinity Biomedical Sciences, Trinity College Dublin, Dublin, Ireland, [2]Department of Mechanical and Manufacturing Engineering, School of Engineering, Trinity College Dublin, Dublin, Ireland, [3]Advanced Materials and Bioengineering Research Centre (AMBER), Royal College of Surgeons in Ireland and Trinity College Dublin, Dublin, Ireland

Received 12 August 2015; accepted 20 November 2015
Published online in Wiley Online Library (wileyonlinelibrary.com). DOI 10.1002/jor.23110

ABSTRACT: The complexity of the in vivo environment makes it is difficult to isolate the effects of specific cues on regulating cell fate during regenerative events such as osteochondral defect repair. The objective of this study was thus to develop a computational model to explore how joint specific environmental factors regulate mesenchymal stem cell (MSC) fate during osteochondral defect repair. To this end, the spontaneous repair process within an osteochondral defect was simulated using a tissue differentiation algorithm which assumed that MSC fate was regulated by local oxygen levels and substrate stiffness. The developed model was able to predict the main stages of tissue formation observed by a number of in vivo studies. Following this, a parametric study was conducted to better understand the dramatic impact on osteochondral healing reported in experimental studies where the rate of angiogenesis was altered. In the simulations where angiogenesis was reduced, by week 12, the subchondral plate was predicted to remain below the native tidemark, although the chondral region was composed entirely of cartilage and fibrous tissue. In the simulations where angiogenesis was increased, more robust cell proliferation and cartilage formation were observed during the first 4 weeks, however, by week 12 the subchondral plate had advanced above the native tidemark although any remaining tissue was either hypertrophic cartilage or fibrous tissue. These results suggest that osteochondral defect repair could be enhanced by interventions where angiogenesis is promoted but confined to within the subchondral region of the defect. © 2015 Orthopaedic Research Society. Published by Wiley Periodicals, Inc. J Orthop Res 9999:1–11, 2015.

Keywords: spontaneous repair; osteochondral defect; computational modeling; angiogenesis; oxygen

Osteochondral defects of a certain size have the capacity to spontaneously repair.[1] This process forms the basis of a number of different treatment strategies for both chondral and osteochondral defect repair.[2,3] The environmental factors regulating this spontaneous repair process however remain poorly understood, with previous computational models suggesting that biomechanical signals may play a key role in directing stem cell fate during osteochondral defect repair.[4] Recently, excessive bone formation during joint regeneration has been linked with vascular invasion of the defect site. Klinger et al.[5] examined the effect of inhibiting angiogenesis within a porcine model of cartilage repair by microfracture. In this study, angiogenesis was inhibited by over expressing the anti-angiogenic factor chondromodulin 1. This resulted in less vascular invasion, an inhibition of chondrocyte hypertrophy and endochondral ossification, as well as more robust hyaline cartilage formation at later time points. Similar results were observed by Nagai et al.[6] within a rabbit model of spontaneous osteochondral defect repair, where administration of an anti-vascular endothelial growth factor was used to inhibit angiogenesis. Both of these studies point to the importance of angiogenesis and associated local oxygen levels in regulating chondrogenesis and endochondral ossification during osteochondral defect repair.

Based on these findings and recent studies which have shown that hypertrophy of chondrocytes is supressed in hypoxic or low oxygen conditions,[7–11] we hypothesized that local oxygen levels are a critical determinant of the success of osteochondral defect repair. It is further hypothesized that limiting angiogenesis within an osteochondral defect improves cartilage repair by inducing a sustained hypoxic environment. To test this, we used a previously developed computational model of MSC differentiation to study the spontaneous repair process within an osteochondral defect. The model was first used to simulate the time-course of healing within an empty defect. Following this, a sensitivity analysis was performed which found that the parameters controlling blood vessel growth and blood vessel branching had the greatest effect on the predicted tissue formation. Finally, a parametric study was conducted to examine how varying these parameters affects tissue formation within an osteochondral defect. The results of these simulations where compared to in vivo studies of OC defect repair under altered angiogenic states.[5,6]

METHOD

Iterative Procedure

Tissue differentiation within the osteochondral defect was simulated via an iterative procedure similar to the one outlined by Burke et al.[1] (Fig. 1 and Supplementary Text 1.1). As part of this, a finite element (FE) model was used to predict the mechanical environment within the defect although an oxygen diffusion model was used to predict the local oxygen tension. The results of these simulations were used as inputs to models of angiogenesis and cell migration, proliferation, death, and differentiation.

Finite Element Model

A simplified 3D FE model of an osteochondral defect within the femoral condyle was constructed using the FE package FEBio (version 2.2.2, University of Utah, Technology Commercialization

Correspondence to: Daniel J. Kelly (T: +353-1-8964214; F: +353-1-6795554; E-mail: kellyd9@tcd.ie)

JOR-15-0490.R1(23110)

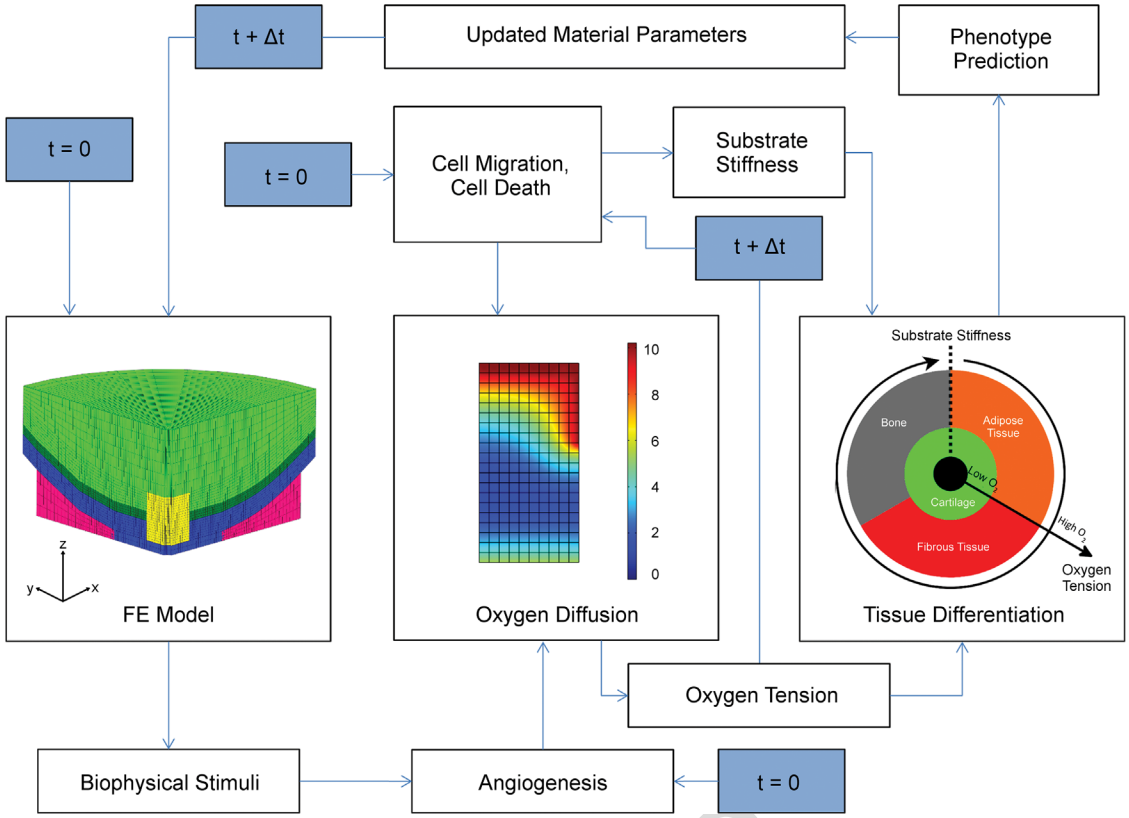

Figure 1. Iterative procedure for the model of the spontaneous repair process within an osteochondral defect.

Office, 615 Arapeen Drive, Suite 310, Salt Lake City). This model was used to predict the biophysical stimuli generated within such a defect during gait (Fig. 2). Similar to previous studies,[4,12,13] the condyle was modeled as a flattened semi-sphere of radius 20 mm which consisted of a 1 mm deep layer of cortical bone which overlaid mature cancellous bone. The condyle was covered with a 2 mm thick layer of cartilage which was supported by the meniscus. The tibial plateau was modeled as a rigid contact layer, the permeability of which was assumed to be the same as cartilage. All materials were modeled as bi-phasic, except for the meniscus which was modeled as a solid elastic material where a sliding interface was used to model the contact between it and the cartilage layer. At the centre of the FE model, a defect of size $\varphi 5\,\text{mm} \times 5\,\text{mm}$ was included. This was assumed to be initially filled with granulation tissue. The material properties of each tissue type are listed in Table 1. A load of 2,400 N was applied over 1 s based on the assumption of five to six times subject weight (80 kg) spread evenly between the lateral and medial compartments.[14]

Model of Angiogenesis

Angiogenesis was modeled using a lattice based approach similar to that outlined by Checa et al. (Fig. 3A).[15] Each lattice point had a diameter of 10 μm which corresponded with an overall lattice density of 1×10^6 lattice points/mm^3. Similar to Checa et al.[15] vessels stopped growing if the

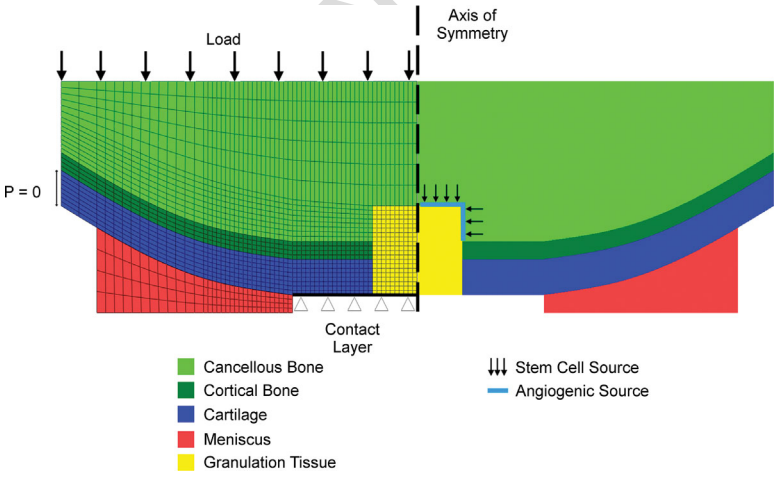

Figure 2. Finite element model of the knee with an osteochondral defect including boundary conditions.

Table 1. Material Properties

Material Property	Granulation Tissue	Fibrous Tissue	Cartilage	Hypertrophic Cartilage	Immature Bone	Mature Bone	Cortical Bone	Meniscus
Young's modulus [MPa]	1[a]	2[a,b]	10[a,b]	20	1,000[a]	6,000[c]	20,000[c]	50
Poisson's ratio	0.167[a]	0.167[a]	0.167[a]	0.167	0.3[a]	0.3[a]	0.3[a]	0.3
Permeability [mm^4/Ns]	0.01[a]	0.01[a,b]	0.005[a,b]	0.005	0.1[a]	0.37[d]	1e-5[a]	–
Solid volume fraction	0.2[a]	0.2[a]	0.2[a]	0.2	0.2[a]	0.2[a]	0.2[a]	–

[a]Lacroix Q3 no Prendergast.[38] [b]Hori and Lewis.[39] [c]Claes et al.[40] [d]Ochoa and Hillberry.[41]

octahedral shear strain exceeded a threshold limit (ε^{angio}) or if anastomosis had occurred. Vessels were also able to branch should their length exceed a certain value (L_{min}). The probability of branching then increased linearly until the vessel reached the maximum allowable length (L_{max}) at which point the probability of branching occurring was 1.[15]

Vessels grew at a constant rate (V^{growth}). Vessel direction was governed using strain dependent rules which were based on the in vitro study conducted by Matsumoto et al.[16] and the corresponding in silico model developed by Burke et al.[17] Briefly, vessel growth was biased in the direction of minimum principal strain whereby there were three potential options in the determination of the vessel direction; (1) continue growing in the previous direction; (2) move in the direction of minimum principal strain or; (3) move in a random direction. The probability that a vessel grew in the same direction as the previous iteration (P^{prev}) was 0.4. The probability that a vessel grew in the direction of the minimum principal strain (P^{strain}) was dependent upon the absolute magnitude of the strain; this was calculated using a simple linear model where $P^{strain}=0$ at $\varepsilon^{min}=0$ up to maximum of $P^{strain}=0.6$ at $|\varepsilon^{min}| \geq 0.18$. The final case where a vessel grew in a random direction was dictated by the remaining probability ($1-P^{prev}-P^{strain}$).

At day 0, it was assumed that vessels grew into the callus from the exposed cancellous bone (Fig. 2). The initial number of vessels was governed by the parameter N^{angio} which denotes the proportion of lattice points on the cancellous bone surfaces which were Q4 invading blood vessels (Table 2).

Cell Migration, Cell Proliferation, and Cell Death

The migration and proliferation of MSCs, osteoblasts (OBs), chondrocytes (CCs), fibroblasts (FBs), and hypertrophic chondrocytes (HC) was also modeled using a lattice approach.[15,18] The migration of cells was implemented using "random walk" theory.[18] Cell proliferation was implemented in a similar fashion. The migration rate (M) determined the number of attempted migration actions per time step although the doubling time (DT) was the required age of a cell before it could proliferate (Table 3). Cell proliferation was inhibited in regions where the oxygen concentration fell below a specific threshold value (O_2^{prolif}) (Table 4). If the oxygen concentration fell below a threshold value (O_2^{death}) then cell death was initiated. The maximum number of cells allowed in any element was limited to 1×10^5 cells/mm.[3,19] It was assumed that 5% of the lattice points on the cancellous surface of the defect (Fig. 2) and 0.5% of the interior lattice points contained MSCs at day 0.

Oxygen Transport

Oxygen transport within the defect was modelled using the FE package COMSOL Multiphysics (version 4.3). The governing equation (Equation 1) was updated during each iteration based on the number of each cell type in a specific element. The oxygen consumption term was updated based on the number of MSCs, CCs, OBs, FBs, and HCs, although the oxygen production term was determined based on the number of ECs (i.e., blood vessels).

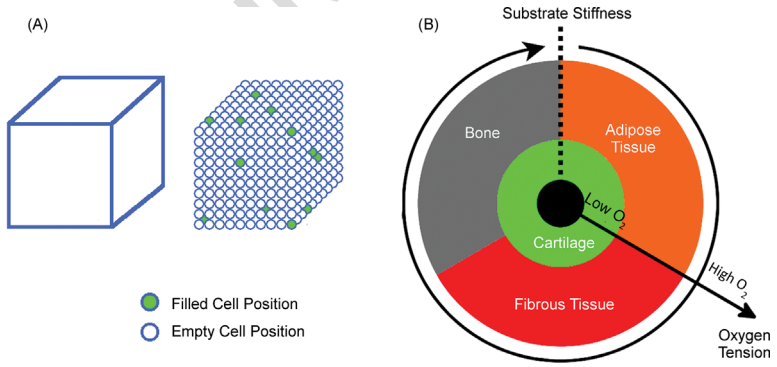

Figure 3. (A) Tissue differentiation algorithm as directed by the local oxygen tension and substrate stiffness. (B) A 3-dimensional finite element with corresponding lattice. Each lattice point represents a potential location for a cell.

Table 2. Angiogenesis and MSC Differentiation Model Parameters

Model Parameter	Symbol	Source	Unit	Value
Octahedral shear strain threshold for inhibition of angiogenesis	ε^{angio}	Estimated	–	0.1
Blood vessel growth rate	V^{growth}	Estimated	$mm\,day^{-1}$	0.1
Minimum length for branching	L_{min}	[15]	mm	0.2
Maximum length without branching	L_{max}	[15]	mm	0.5
Minimum cell age for MSC differentiation	Age^{cell}	Estimated	days	5
Oxygen diffusion coefficient	G	[19,42]	$mm^2\,s^{-1}$	2.2E-03
Initial oxygen tension	$O_2{}^{initial}$	[43]	$mol\,mm^{-3}$	101.6E-12
Oxygen tension for inhibition of differentiation	$O_2{}^{inhibition}$	[44]	$mol\,mm^{-3}$	5E-12
Oxygen limit for cartilage	$O_2{}^{cartilage}$	[19]	$mol\,mm^{-3}$	30E-12
Oxygen limit for differentiation of cartilage to hypertrophic cartilage	$O_2{}^{hypertrophic}$	Estimated	$mol\,mm^{-3}$	30E-12
Oxygen limit for calcification of hypertrophic cartilage	$O_2{}^{endochondral}$	Estimated	$mol\,mm^{-3}$	50.48E-12

$$\frac{dO_2}{dt} = G\nabla^2 O_2 - \sum_{n=1}^{6} \rho^n \frac{Q^{max,n} O_2}{K^{m,n} + O_2} + Q^{vessels} \quad (1)$$

The oxygen diffusion coefficient $G = 2.2 \times 10^{-3}\ mm^2 s^{-1}$. Oxygen consumption was modeled separately for each cell phenotype using Michealas-Menten kinetics.[20–22] In the equation shown each phenotype was represented by n (Table 4). For each cell type; ρ^n was the number of cells in the element; $Q^{max,n}$ was the maximum oxygen consumption and; $K^{m,n}$ was the oxygen consumption at half maximum concentration.

The oxygen supply from the blood vessels within each element was described using $Q^{vessels}$, which was calculated using the relationship in Equation (2).

$$Q^{vessels} = \begin{cases} \dfrac{O_2^{vessels} - O_2}{K^{vessels}}, & O_2 < O_2{}^{vessels} \\ 0, & O_2 \geq O_2{}^{vessels} \end{cases} \quad (2)$$

$K^{vessels}$ was a temporal smoothing term used to prevent irregular jumps in the oxygen concentration ($K^{vessels} = 10\,s$). $O_2{}^{vessels}$ was the minimum allowable oxygen concentration within the element. $O_2{}^{vessels}$ was determined as a function of $v^{density}$, which was the percentage of lattice points within the element containing ECs. A linear relationship was used to calculate $O_2{}^{vessels}$ where $O_2{}^{vessels} = 0\,mol/mm^3$ for $v^{density} = 0$ up to a maximum of $O_2{}^{vessels} = 101.6 \times 10^{-12}\,mol/mm^3$ at $v^{density} = v^{density,\,max}$.

It was assumed that there was a constant oxygen tension of $101.6 \times 10^{-12}\,mol/mm^3$ (10%) at the exposed bone within the defect. Furthermore, a constant oxygen boundary condition of $50.80 \times 10^{-12}\,mol/mm^3$ (5%) was applied to the surface of the defect in order to simulate the nutrient supply from the synovial fluid.[22] Finally, the following three assumptions were made.[22] (i) The synovial fluid was well mixed and as such any gradients were negligible. (ii) Oxygen transport was steady state meaning that the effects of mechanical loading and cartilage deformation on oxygen transport were ignored. (iii) Gradients from the cell surface to the bulk tissue were negligible.

Table 3. Cell Model Parameters

Model Parameter	MSC	CC	OB	FB	HC
Doubling time [days]	0.5[a]	1.5[a]	1[a]	0.5[a]	1.5[a]
Migration rate [μm/h]	26.6[c]	N/A	N/A	26.6[c]	N/A
Anoxic death rate [% cells day^{-1}]	20	20	20	20	20

[a]Isaksson et al.[45] [b]Burke et al.[33] [c]Appeddu and Shur[46]

MSC Differentiation

The rules governing MSC differentiation are outlined in detail elsewhere[19] and are graphically depicted in Figure 3B (Supplementary Text 1.2). As adipogenesis is not observed in the early stages of osteochondral defect repair it was excluded from the model based on the assumption that the stiffness of the granulation tissue was not low enough to facilitate it.

Endochondral ossification was modeled as a two-step process which first involved CCs becoming hypertrophic before ossification of the tissue began.[23] It was assumed that chondrocyte hypertrophy occurred in regions where the oxygen tension increased beyond a threshold value ($O_2{}^{hypertrophic}$).[8,10,24] Following this, the second step depicted the ossification process whereby HCs either transdifferentiate into, or are replaced by invading OBs.[23,25] In this model, HCs were replaced with OBs provided that (1) they were in an element where the oxygen tension was greater than a threshold value ($O_2{}^{endochondral}$) and (2) they were in the vicinity of an OB.

Simulations

The spontaneous repair process was simulated over a period of 12 weeks where each iteration represented a time period of 24 h. Using the estimated parameters, a model of the spontaneous repair process within an untreated empty defect was simulated. The results of this simulation were then used as the baseline for a sensitivity analysis which was conducted on each of the estimated parameters (Table 5). Similar to Carlier et al.,[26] each parameter was varied between 50% and 150% of its estimated value. At the end of each simulation the predicted quantity of each tissue type was compared to the baseline model. Following this, the effect of reducing and increasing the rate of angiogenesis within an osteochondral defect was examined by performing a parametric study where the parameters controlling the blood vessel growth rate (V^{growth}) and the branching rate (L^{min} & L^{max}) were varied with respect to the values used in the baseline model.

Table 4. Oxygen Parameters For Each Cell Phenotype

Michealas–Menten Coefficients	MSC	CC	OB	FB	HC
Cell type (n)	1	2	3	4	5
Max consumption rate (Q^{max}) [mol cell^{-1} h^{-1}]	93.2×10^{-15a}	$1.8 \times 10^{-15a,b}$	93.2×10^{-15a}	93.2×10^{-15a}	1.8×10^{-15a}
Oxygen concentration at half max consumption [mol mm^{-3}]	22.5×10^{-12}	22.5×10^{-12}	22.5×10^{-12}	22.5×10^{-12}	22.5×10^{-12}
Oxygen concentration for cell proliferation (O_2^{prolif}) [mol mm^{-3}]	40×10^{-12a}	10×10^{-12}	80×10^{-12a}	20×10^{-12}	30×10^{-12}
Oxygen concentration for cell death (O_2^{death}) [mol mm^{-3}]	5×10^{-12c}	5×10^{-12a}	20×10^{-12a}	5×10^{-12}	5×10^{-12a}

[a]Carlier et al.[26] [b]Malda et al.[47] [c]Zhu et al.[7]

RESULTS

Untreated Osteochondral Defect

At day 0, although the defect was predicted to be devoid of vessels (Fig. 4A), the oxygen tension in the base (Fig. 4B) was high as a result of the constant oxygen boundary condition at the exposed cancellous bone. Within the first 2 weeks an anoxic environment was predicted in the core of the defect, which resulted in reduced cell viability in this region. Cell proliferation was confined mainly to the base, although some proliferation was observed at the defect surface due to the oxygen supply from the synovial fluid. By day 14, osteogenesis was predicted at the exposed bone, however as the majority of the subchondral region was hypoxic, most of the MSCs in this region differentiated into chondrocytes (Fig. 4C). Conversely, at the surface of the defect the more normoxic environment resulted in the formation of fibrous tissue with cartilage directly

Table 5. Results of the Sensitivity Analysis

Parameter	Symbol	Value	Granulation Tissue [%]	Bone [%]	Fibrous Tissue [%]	Cartilage [%]	Hypertrophic Cartilage [%]
Baseline (untreated defect)			0	78	5	0	17
Initial proportion of lattice points which are assigned active blood vessels [%]	N^{angio}	7.5	0	78	5	0	17
		22.5	0	77	5	0	18
Proportion of lattice points in an element which must contain vessels for it to be fully vascularised	$V^{density,max}$	0.1	0	83	5	0	12
		0.3	0	72	5	0	22
Blood vessel growth rate [mm/day]	V^{growth}	0.06	1	47	4	38	10
		0.14	0	84	1	0	15
Strain threshold for inhibition of angiogenesis [%]	ε^{angio}	5	0	72	5	12	10
		15	0	78	5	0	17
Oxygen tension required for hypertrophy [%]	$O_2^{hypertrophy}$	1	0	76	5	0	19
		5	0	74	5	14	7
Oxygen tension required for endochondral ossification [%]	$O_2^{endochondral}$	3	1	81	5	0	14
		7	0	76	5	0	19
Minimum and maximum length for blood vessel branching [mm]	L^{min} & L^{max}	0.1–0.3	0	88	2	0	10
		0.3–0.7	0	58	5	23	14
Young's modulus of the meniscus [MPa]	$E^{meniscus}$	25	1	76	5	0	19
		75	0	73	5	5	17
Required age of a cell before it has produced enough matrix to influence the neighbouring cells [days]	$Age^{changed}$	1	0	79	5	0	16
		5	0	68	5	0	27

The percentage of each tissue type is measured at day 84 and the standard condition is indicated in bold.

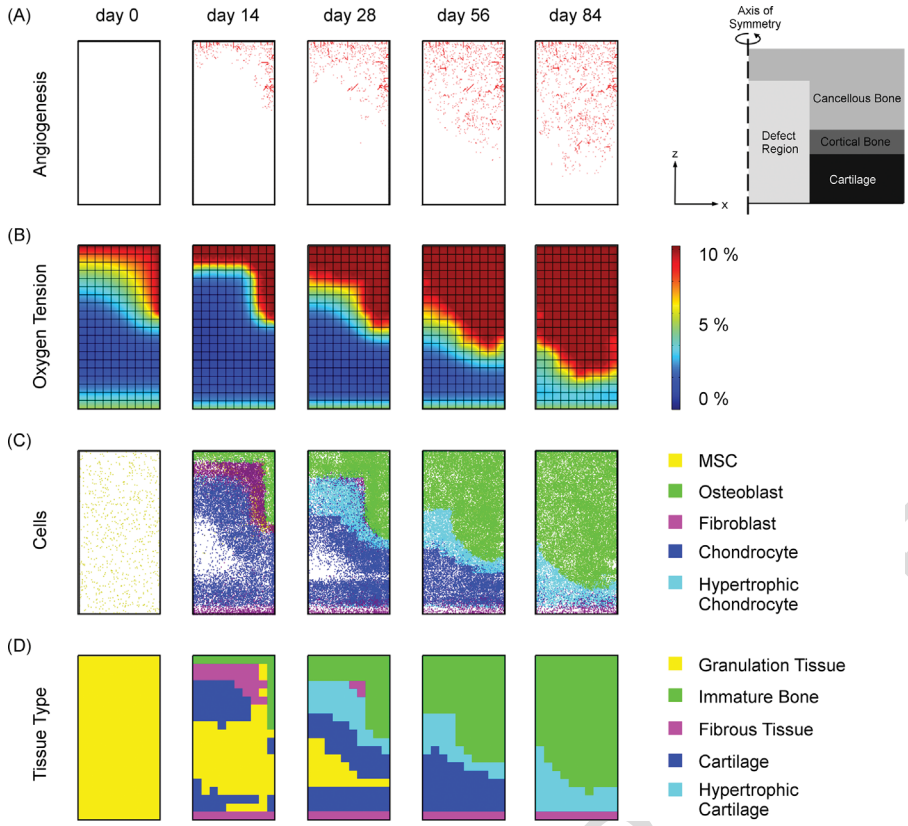

Figure 4. Predicted pattern of (A) angiogenesis, (B) oxygen tension, (C) cell differentiation, and (D) tissue type during the spontaneous repair of an osteochondral defect at day 0, 14, 28, 56, and 84.

below it (Fig. 4D). By day 28, as blood vessels penetrated further into the defect, a normoxic environment formed which resulted in the cartilage in the base becoming hypertrophic. As this was converted to bone by endochondral ossification, the subchondral plate advanced towards the surface of the defect. By day 35 (data not shown), all of the granulation tissue had been replaced. The quantity of cartilage (39%) peaked at this time and steadily decreased as it underwent hypertrophy and was replaced with bone by endochondral ossification. By day 56 the advancing bone formed in an infundibuliform (funnel) shape as it approached the chondral region (Fig. 4C). At this time point the majority of the tissue within the chondral region remained as cartilage (Fig. 4D). By day 84 however, the subchondral plate had advanced above the tidemark and all of the cartilage had become hypertrophic (Fig. 4D).

Sensitivity Analysis

The majority of the estimated parameters had very little influence on the final prediction of each tissue type (Table 5). Regarding these, varying each parameter by ±50% of its estimated value resulted in a deviation of, at most, ±10 percentage points from the predicted quantity of each tissue within the baseline simulation. The exceptions to this were the parameters $\varepsilon^{\text{angio}}$, $O_2{}^{\text{Hypertrophy}}$, V^{growth}, and L^{min} & L^{max}. In the case of the first two, altering these parameters affected the amount of cartilage which was hypertrophic at day 84. The latter two parameters influenced the degree of vascularization within the defect which in turn regulated the oxygen concentration. Varying these thus affected both the rate at which cartilage became hypertrophic and the rate at which hypertrophic cartilage was converted to bone by endochondral ossification. In this case, either decreasing the blood vessel growth rate, or increasing the branching limits, decreased the predicted quantity of bone and hypertrophic cartilage at day 84. Conversely, increasing the blood vessel growth rate, or decreasing the vessel branching limits, enhanced the effect of angiogenesis which in turn increased the predicted quantity of bone at day 84.

Influence of Angiogenesis on Osteochondral Defect Repair

Varying the model parameters controlling the blood vessel growth rate (V^{growth}) and the rate of vessel branching (L^{min} & L^{max}) had different effects on the predicted pattern of angiogenesis (Fig. 5 and S-Movies 1–9). Altering the vascular growth rate changed the time it took vessels to progress from the cancellous bone to the surface of the defect. When this parameter was high (relative to the baseline simulation), blood vessels had filled the defect by day 56 (Fig. 5C). When it was low blood vessels only began to form within the

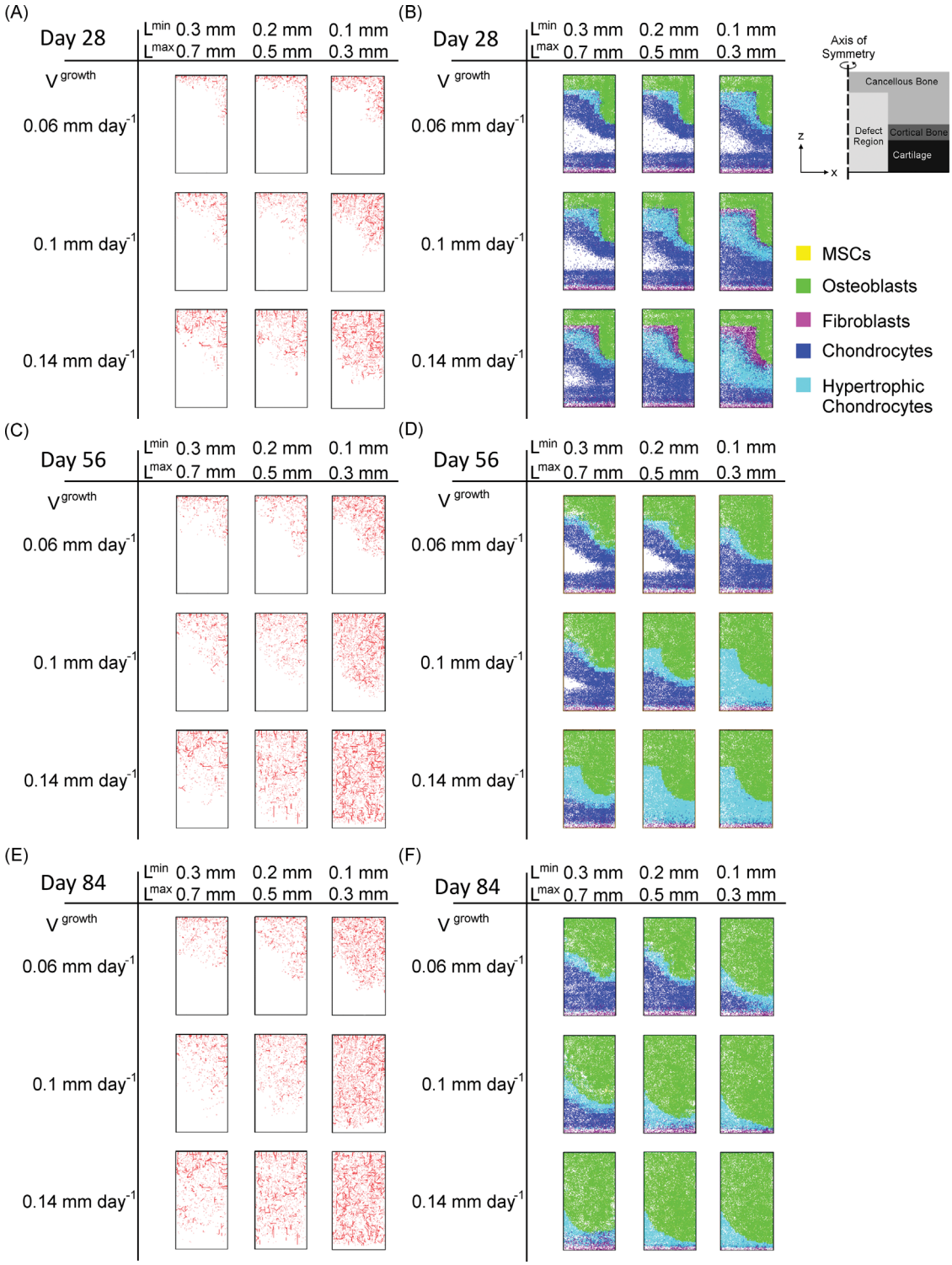

Figure 5. Results of the parametric study where V^{growth} and L^{min} & L^{max} are varied with respect to their respective baseline values (V^{growth}, baseline = 0.1 mm day-1; L^{min}, baseline = 0.2 mm and L^{max}, baseline = 0.5 mm). The predicted angiogenesis and cell phenotype within the defect are shown for (A, B) day 28, (C, D) day 56, and (E, F) day 84.

chondral phase by day 84 (Fig. 5E). Conversely, changing the rate of branching affected the density of vessels within a vascularized region. They did not however affect the distance that blood vessels were predicted to have progressed. When these limits were low (relative to the baseline values) the rate of branching increased and when they were high the rate of branching decreased.

Changing the parameters controlling angiogenesis had a large effect on the predicted patterns of MSC differentiation and tissue formation. At day 28 however tissue formation in all of the simulations followed

the same general trend (Fig. 5B) where bone formed by intramembranous ossification in the base of the defect and fibrous tissue formed at the surface. Interestingly, regardless of the angiogenic parameters, roughly the same quantity of bone was predicted across all of the simulations at this time point. The simulations differed however regarding the type of tissue forming in the core of the defect. When either the vessel growth or the branching rates were low, a region which was almost devoid of cells was predicted in the core. The size of this core increased when both rates were low. Conversely, when either of the angiogenic rates was high, and the other was at its respective baseline value, this hypocellular region did not form. Instead FBs and HCs were predicted above the bone in the osseous region while the chondral region was almost entirely filled with CCs. When both parameters were high, CCs became hypertrophic in the chondral region by day 28.

Similar trends were predicted at day 56 (Fig. 5D) and day 84 (Fig. 5F). At day 56, in all simulations, bone continued to form in the osseous region although FBs remained at the surface. In the simulations where either of the vascular growth or the branching rates were low a hypocellular core remained, however this was smaller than in the day 28 simulations. Similar results were obtained when both rates were low. At day 84, in these groups bone did not progress beyond the native subchondral plate and the majority of the chondral region was predicted to be cartilage. Conversely in the simulations where either or both of the angiogenic rates were high all of the chondrocytes in the defect became hypertrophic. This behavior continued and by day 84, the majority of the chondral region was bone.

DISCUSSION

The objective of this study was firstly to test if the temporal and spatial patterns of tissue differentiation observed during OC defect repair could be simulated using a computational model where MSC fate was hypothesized to be regulated by local oxygen levels and substrate stiffness. The second objective was to use this computational model to examine how varying the rate of angiogenesis affects the progression of tissue formation during OC defect repair over a 12 week period. A baseline simulation was first performed which used estimated parameters to predict the spontaneous repair process within an untreated osteochondral defect. A sensitivity analysis was then conducted on these parameters in order to examine their influence on the predicted quantities of each tissue type. The results from this highlighted the extent of the effect that angiogenesis, and in particular the rates of vascular growth and vessel branching, had on the spontaneous repair process. In the final part of this study, the role of angiogenesis was further examined by varying the key angiogenic parameters in the model. These simulations suggest that control of angiogenesis is critical to successful osteochondral defect repair.

The computational model was able to predict the main features of osteochondral defect repair reported in a number of different animal models. During the first 2 weeks of repair, similar to that observed experimentally by DePalma et al.,[27] cell proliferation was mainly confined to the base of the defect. By day 14, distinct cellular zones were observed, with OBs predicted in the base, CCs above these and FBs at the surface. This early spatial pattern has been described in numerous animal models.[1,28,29] As the simulation progressed, the newly formed osseous tissue advanced towards the surface as cartilage was converted to bone by endochondral ossification. This advancement of subchondral bone is one of the main features of osteochondral defect repair.[1,28,30,31] In addition to this, the model was able to predict the early pattern of bone formation observed by Orth et al.[30] In the simulation, at 3 weeks, bone formation took on a cylindrical shape where very little immature bone was observed (data not shown).[30] At day 42 however, bone formation had increased and adopted an infundibuliform shape.[30] Furthermore, as observed in the literature, by day 56, the subchondral plate remained below the native tidemark.[30,31] Finally, by week 12, the subchondral plate was predicted to have progressed above the tidemark although only hypertrophic cartilage remained within the defect.[6]

The model predictions of spontaneous repair where the rate of angiogenesis was lowered also agreed with the main findings observed by Nagai et al.[6] In their study, defects which were treated with the anti-angiogenic factor bevacizumab displayed similar patterns of healing to untreated controls at day 28, behavior which was also predicted in the simulations. Furthermore, similar to Nagai et al.,[6] at this time-point the predominant tissue predicted within the model was cartilage. At week 12 however, Nagai et al.[6] reported marked differences in the observed pattern of healing between the untreated control group and the bevacizumab treated group. In this case, control defects consisted mainly of bone and fibrous tissue with no evidence of cartilage tissue persisting. This was also predicted in the baseline simulation, where bone penetrated above the native tidemark, although any remaining cartilage had become hypertrophic. In contrast, in the bevacizumab treated group, Nagai et al.[6] reported that a large portion of the tissue retained its chondrogenic phenotype, although bone formation was restricted to the base of the defect. This was also observed within the reduced angiogenesis simulations where the majority of the chondral region was composed of cartilage and the majority of the subchondral region was composed of bone. These similarities between the model predictions and the in vivo results provide support for the underlying model hypotheses regarding the role of oxygen levels in regulating MSC fate during OC defect

repair. In particular, the results of this study provide support for the hypothesis that limiting angiogenesis to the osseous region of an osteochondral defect will improve cartilage repair by inducing a sustained hypoxic environment in the chondral region.

In the simulations where the rate of angiogenesis was upregulated more robust tissue formation was predicted during the first 4 weeks compared to the other models. In this case, by day 28, although bone formation was approximately the same, increasing the rate of angiogenesis led to greater cell proliferation and an increase in the quantity of cartilage observed within the chondral phase. As this model progressed however, the higher rate of angiogenesis resulted in early blood vessel growth into the chondral region. This generated a normoxic environment and by day 56 the newly formed cartilage had become hypertrophic. These results suggest that during osteochondral defect repair, robust tissue formation can be induced by promoting and inhibiting angiogenesis within the subchondral and chondral regions respectively. It is interesting to note that within a rabbit model, in osteochondral defects treated with a bioabsorbable scaffold which induced regeneration of the cartilage tissue in the superficial layer, the pro-angiogenic factor VEGF was localized in the subchondral region of the defect.[32] In the same study, in untreated defects VEGF was localized throughout the entire defect and no cartilage regeneration was observed.[32]

One of the main issues with the current model was that it was unable to predict the spatial patterns of bone formation which were observed during the later stages of the spontaneous repair process by Orth et al.[30] Orth et al.[30] reported that as the subchondral plate advances towards the native tidemark it changes from an infundibuliform shape, becomes plane with the native cortical bone before adopting a convex pattern as it progresses into the chondral region. In all of the developed models however, the osseous tissue retained this infundibuliform shape as it formed above the native tidemark. There are a number of potential reasons for this which will be addressed in future work. Firstly, the current model was developed based on the findings of Burke et al.[19,33,34] who hypothesized that mechanical loading plays an indirect role upon tissue formation by affecting the course of blood vessel growth. In this study we found that determining blood vessel direction using a random function, rather than with a strain dependent algorithm,[17] had only a small effect on the predicted outcome of tissue formation (Supplementary Text 1.3, Figs. S1 and S2). Based on this, we speculate that, within an osteochondral defect, the mechanical environment also has a direct influence on tissue formation by affecting the quality of the cartilage tissue as well as the course of endochondral ossification. Another feature which will be addressed in future work is that the current model did not differentiate between hyaline cartilage and fibrocartilage. This is necessary as fibrocartilage has been observed to form in the chondral region of the defect.[5,6,29,35,36] Furthermore, it has been hypothesized that the eventual degradation of the repair tissue is caused by differences in the biomechanical properties of these two tissues.[37]

There were a number of other limitations associated with the computational model which may have limited its predictive capacity. Firstly, a simplified finite element model of the femoral condyle was developed where each tissue type was described using as an isotropic elastic material. We are satisfied however that the current approach sufficiently described the mechanical environment within the osteochondral defect. In addition to this, although similar studies to ours have modeled the meniscus as a biphasic, anisotropic material,[4,12] in this study it was characterized as an isotropic elastic material. The results of a sensitivity analysis however confirm that the final model predictions were reasonably insensitive to the estimated stiffness of the meniscus.

In spite of these limitations the current model was able to predict the main features and differences observed during both spontaneous and angiogenically impaired repair within an osteochondral defect. Based on these results it was possible to determine the mechanism by which limiting blood vessel growth during osteochondral defect repair improves the quality of the repair tissue. In addition to this the current study provides support for the hypotheses that MSC differentiation is governed by both the substrate stiffness and oxygen tension and that chondrocyte hypertrophy is initiated in a normoxic environment. Future work will involve updating the current model to improve its capacity to accurately predict the spatial patterns of tissue formation observed during the later stages of the spontaneous repair process.

AUTHORS' CONTRIBUTIONS

A.O.R. developed the computational model and performed the simulations. D.K. critically revised the paper and approved the final submitted version. All authors have read and approved the final submitted draft.

REFERENCES

1. Shapiro F, Koide S, Glimcher MJ. 1993. Cell origin and differentiation in the repair of full-thickness defects of articular cartilage. J Bone Jt Surg 75-A:532–553.
2. Nukavarapu SP, Dorcemus DL. 2013. Osteochondral tissue engineering: current strategies and challenges. Biotechnol Adv 31:706–721.
3. Panseri S, Russo A, Cunha C, et al. 2012. Osteochondral tissue engineering approaches for articular cartilage and subchondral bone regeneration. Knee Surg Sports Traumatol Arthrosc 20:1182–1191.
4. Kelly DJ, Prendergast PJ. 2005. Mechano-regulation of stem cell differentiation and tissue regeneration in osteochondral defects. J Biomech 38:1413–1422.
5. Klinger P, Surmann-Schmitt C, Brem M, et al. 2011. Chondromodulin 1 stabilizes the chondrocyte phenotype and

inhibits endochondral ossification of porcine cartilage repair tissue. Arthritis Rheum 63:2721–2731.
6. Nagai T, Sato M, Kutsuna T, et al. 2010. Intravenous administration of anti-vascular endothelial growth factor humanized monoclonal antibody bevacizumab improves articular cartilage repair. Arthritis Res Ther 12:R178.
7. Zhu M, Feng Q, Bian L. 2014. Differential effect of hypoxia on human mesenchymal stem cell chondrogenesis and hypertrophy in hyaluronic acid hydrogels. Acta Biomater 10:1333–1340.
8. Sheehy EJ, Buckley CT, Kelly DJ. 2012. Oxygen tension regulates the osteogenic, chondrogenic and endochondral phenotype of bone marrow derived mesenchymal stem cells. Biochem Biophys Res Commun 417:305–310.
9. Leijten JCH, Moreira Teixeira LS, Landman EBM, et al. 2012. Hypoxia inhibits hypertrophic differentiation and endochondral ossification in explanted tibiae. PLoS ONE 7: e49896.
10. Leijten J, Georgi N, Moreira Teixeira L, et al. 2014. Metabolic programming of mesenchymal stromal cells by oxygen tension directs chondrogenic cell fate. Proc Natl Acad Sci USA http://www.ncbi.nlm.nih.gov/pubmed/25205812
11. Gawlitta D, van Rijen MHP, Schrijver EJM, et al. 2012. Hypoxia impedes hypertrophic chondrogenesis of human multipotent stromal cells. Tissue Eng Part A 18:1957–1966.
12. Wilson W, Van Rietbergen B, Van Donkelaar CC, et al. 2003. Pathways of load-induced cartilage damage causing cartilage degeneration in the knee after meniscectomy. J Biomech 36:845–851.
13. Vaziri A, Nayeb-Hashemi H, Singh A, et al. 2008. Influence of meniscectomy and meniscus replacement on the stress distribution in human knee joint. Ann Biomed Eng 36:1335–1344.
14. Shirazi R, Shirazi-Adl a. 2009. Computational biomechanics of articular cartilage of human knee joint: effect of osteochondral defects. J Biomech 42:2458–2465.
15. Checa S, Prendergast PJ. 2009. A mechanobiological model for tissue differentiation that includes angiogenesis: a lattice-based modeling approach. Ann Biomed Eng 37:129–145.
16. Matsumoto T, Yung YC, Fischbach C, et al. 2007. Mechanical strain regulates endothelial cell patterning in-vitro. Tissue Eng 13:207–217.
17. Burke DP, Kelly DJ. 2014. A mechanobiological model of endothelial cell migration and proliferation. Comput Methods Biomech Biomed Engin.
18. Pérez Ma, Prendergast PJ. 2007. Random-walk models of cell dispersal included in mechanobiological simulations of tissue differentiation. J Biomech 40:2244–2253.
19. Burke DP, Kelly DJ. 2012. Substrate stiffness and oxygen as regulators of stem cell differentiation during skeletal tissue regeneration: a mechanobiological model. PLoS ONE 7: e40737.
20. Sengers BG, van Donkelaar CC, Oomens CWJ, et al. 2005. Computational study of culture conditions and nutrient supply in cartilage tissue engineering. Biotechnol Prog 21:1252–1261.
21. Heywood HK, Knight MM, Lee a D. 2010. Both superficial and deep zone articular chondrocyte subpopulations exhibit the Crabtree effect but have different basal oxygen consumption rates. J Cell Physiol 223:630–639.
22. Zhou S, Cui Z, Urban JPG. 2004. Factors influencing the oxygen concentration gradient from the synovial surface of articular cartilage to the cartilage-bone interface: a modeling study. Arthritis Rheum 50:3915–3924.
23. Mackie EJ, Ahmed a Y, Tatarczuch L, et al. 2008. Endochondral ossification: how cartilage is converted into bone in the developing skeleton. Int J Biochem Cell Biol 40:46–62.
24. Ma T, Grayson WL, Frohlich M, et al. 2009. Hypoxia and stem cell-based engineering of mesenchymal tissues. Biotechnol Prog 25:32–42.
25. Bahney C, Hu D, Ferro F, et al. 2014. Transdifferentiation of hypertrophic chondrocytes during endochondral bone repair by activation of pluripotent stem cell programs (216.1). J Fed Am Soc Exp Biol 28.
26. Carlier A, Geris L, Gastel Van N, et al. 2015. Oxygen as a critical determinant of bone fracture healing—a multiscale model. J Theor Biol 365:247–264.
27. DePalma AF, McKeever CD, Subin DK. 1966. Process of repair of articular cartilage demonstrated by histology and autoradiography with tritiated thymidine. Clin Orthop Relat Res 48:229–242.
28. Harada Y, Tomita N, Nakajima M, et al. 2005. Effect of low loading and joint immobilization for spontaneous repair of osteochondral defect in the knees of weightless (tail suspension) rats. J Orthop Sci 10:508–514.
29. Metsaranta M, Kujala UM, Pelliniemi L, et al. 1996. Evidence for insufficient chondrocytic differentiation during repair of full-thickness defcts of articular cartilage. Matrix Biol 15:39–47.
30. Orth P, Cucchiarini M, Kaul G, et al. 2012. Temporal and spatial migration pattern of the subchondral bone plate in a rabbit osteochondral defect model. Osteoarthr Cartil 20:1161–1169.
31. Qui YS, Shahgaldi BF, Revell WJ, et al. 2003. Observations of subchondral plate advancement during osteochondral repair: a histomorphometric and mechanical study in the rabbit femoral condyle. Osteoarthr Cartil 11:810–820.
32. Sakata R, Kokubu T, Nagura I, et al. 2012. Localization of vascular endothelial growth factor during the early stages of osteochondral regeneration using a bioabsorbable synthetic polymer scaffold. J Orthop Res 252–259.
33. Burke D, Dishowitz M, Sweetwyne M, et al. 2013. The role of oxygen as a regulator of stem cell fate during fracture repair in TSP2-null mice. J Orthop Res 31:1585–1596.
34. Burke DP, Khayyeri H, Kelly DJ. 2014. Substrate stiffness and oxygen availability as regulators of mesenchymal stem cell differentiation within a mechanically loaded bone chamber. Biomech Model Mechanobiol http://www.ncbi.nlm.nih.gov/pubmed/24832965
35. Gotterbarm T, Breusch SJ, Schneider U, et al. 2008. The minipig model for experimental chondral and osteochondral defect repair in tissue engineering: retrospective analysis of 180 defects. Lab Anim 42:71–82.
36. Jackson DW, Lalor PA, Aberman HM, et al. 2001. Spontaneous repair of full-thickness defects of articular cartilage in a goat model. J Bone Jt Surg 83-A:53–64.
37. Ochi M, Uchio Y, Tobita M, et al. 2001. Current concepts in tissue engineering technique for repair of cartilage defect. Artif Organs 25:172–179.
38. Lacroix D, Prendergast PJ. 2002. A mechano-regulation model for tissue differentiation during fracture healing: analysis of gap size and loading. J Biomech 35:1163–1171.
39. Hori RY, Lewis JL. 1982. Mechanical properties of the fibrous tissue found at the bone-cement interface following total joint replacement. J Biomed Mater Res 16:911–927.
40. Claes LE, Heigele a C, Neidlinger-Wilke C, et al. 1998. Effects of mechanical factors on the fracture healing process. Clin Orthop Relat Res S132–S147.
41. Ochoa JA, Hillberry BM. 1992. Permeability of bovine cancellous bone. Trans 38th ORS 162.
42. Hershey D, Karhan T. 1968. Diffusion coefficients for oxygen transport in whole blood. AIChE 14:969–972.
43. Epari DR, Lienau J, Schell H, et al. 2008. Pressure, oxygen tension and temperature in the periosteal callus during bone healing—an in vivo study in sheep. Bone 43:734–739.

44. Holzwarth C, Vaegler M, Gieseke F, et al. 2010. Low physiologic oxygen tensions reduce proliferation and differentiation of human multipotent mesenchymal stromal cells. BMC Cell Biol 11. http://www.biomedcentral.com/1471-2121/11/11
45. Isaksson H, van Donkelaar CC, Huiskes R, et al. 2008. A mechano-regulatory bone-healing model incorporating cell-phenotype specific activity. J Theor Biol 252:230–246.
46. Appeddu PA, Shur BD. 1994. Molecular analysis of cell surface fi-1, 4-galactosyltransferase function during cell migration. Proc Natl Acad Sci 2095–2099.
47. Malda J, Rouwkema J, Martens DE, et al. 2004. Oxygen gradients in tissue-engineered PEGT/PBT cartilaginous constructs: measurement and modeling. Biotechnol Bioeng 86:9–18.

SUPPORTING INFORMATION

Additional supporting information may be found in the online version of this article at the publisher's website.

AUTHOR QUERY FORM

JOURNAL: JOURNAL OF ORTHOPAEDIC RESEARCH

Article: jor23110

Dear Author,

During the copyediting of your paper, the following queries arose. Please respond to these by annotating your proofs with the necessary changes/additions using the E-annotation guidelines attached after the last page of this article.

We recommend that you provide additional clarification of answers to queries by entering your answers on the query sheet, in addition to the text mark-up.

Query No.	Query	Remark
Q1	A running head short title was not supplied; please check if this one is suitable and, if not, please supply a short title of up to 45 characters that can be used instead.	
Q2	Please confirm that given names (red) and surnames/family names (green) have been identified correctly.	
Q3	Please check the presentation of table footnote.	
Q4	Table 2 was not cited in the text. An attempt has been made to insert the table into a relevant point in the text, please check that this is OK. If not, please provide clear guidance on where it should be cited in the text.	
Q5	Please provide link for footnote (b) in table 3.	
Q6	Please check the presentation of table footnote.	
Q7	Please check the presentation of table footnote.	
Q8	Please provide the page range and the volume number.	
Q9	Please provide the page range and the volume number.	
Q10	Please provide the volume number.	
Q11	Please provide the page range and the volume number.	
Q12	Please update.	
Q13	Please provide the volume number.	
Q14	Please provide the page range.	

WILEY

COLOR REPRODUCTION IN YOUR ARTICLE

Color figures were included with the final manuscript files that we received for your article. Because of the high cost of color printing, we can only print figures in color if authors cover the expense.

Please indicate if you would like your figures to be printed in color or black and white. Color images will be reproduced online in *Wiley Online Library* at no charge, whether or not you opt for color printing.

Failure to return this form will result in the publication of your figures in black and white.

JOURNAL **JOURNAL OF ORTHOPAEDIC RESEARCH** VOLUME _____ ISSUE _____

TITLE OF MANUSCRIPT _____

MS. NO. _____ NO. OF COLOR PAGES _____ AUTHOR(S) _____

No. Color Pages	Color Charges	No. Color Pages	Color Charges	No. Color Pages	Color Charges
1	400	5	2000	9	3600
2	800	6	2400	10	4000
3	1200	7	2800	11	4400
4	1600	8	3200	12	4800

Please contact the Production Editor for a quote if you have more than 12 pages of color

☐ Please print my figures in black and white

☐ Please print my figures in color

BILL TO:
Name _____ **Purchase Order No.** _____

Institution _____ Phone _____

Address _____

_____ Fax _____

_____ E-mail _____